ELSEVIER

Biomaterials 23 (2002) 2211–2220

Biomaterials

www.elsevier.com/locate/biomaterials

Nucleation of biomimetic Ca–P coatings on Ti6Al4V from a SBF × 5 solution: influence of magnesium

F. Barrere[a,b,*], C.A van Blitterswijk[a,b], K. de Groot[a,c], P. Layrolle[a]

[a] *IsoTis BV, PO Box 98, 3720 AB Bilthoven, Netherlands*
[b] *Twente University, Netherlands*
[c] *Leiden University, Netherlands*

Received 15 February 2001; accepted 12 October 2001

Abstract

Biomimetic Calcium–Phosphate (Ca–P) coatings were applied by using 5 times concentrated Simulated Body Fluid (SBF × 5) using Carbon Dioxide gas. This process allows the deposition of a uniform Ca–P coating within 24 h. A previous study of our process emphasized the importance of hydrogenocarbonate ions (HCO_3^-), a crystal growth inhibitor. The aim of the present study was to investigate the role of the other crystal growth inhibitor present in SBF × 5, Magnesium (Mg^{2+}), on the Ca–P coating formation. Several SBF × 5 solutions were prepared with various Mg^{2+} and HCO_3^- contents. No Ca–P deposits were detected on Ti6Al4V substrate soaked for 24 h in a Mg-free SBF × 5 solution, whereas by increasing HCO_3^- content in a Mg-free SBF × 5 solution, a Ca–P coating developed on Ti6Al4V substrate. Therefore, it appeared that Mg^{2+} has a stronger inhibitory effect on apatite crystal growth than HCO_3^-. Nevertheless, Mg^{2+} plays also another important role as suggested by depth profile X-ray Photoelectron Spectroscopy (XPS) of the Ca–P coating obtained from SBF × 5 solution. Ca^{2+} and Mg^{2+} contents increased significantly at the titanium/coating interface. Therefore, Ca^{2+} and Mg^{2+} initiated Ca–P coating from SBF × 5 solution. The relatively high interfacial concentration in Mg^{2+} favors heterogeneous nucleation of tiny Ca–P globules onto the substrate. So physical adhesion is enhanced at the early stage of the coating formation.

Keywords: Biomimetic; Calcium–Phosphate; Coating; Carbon dioxide; Magnesium; Titanium

1. Introduction

Biomimetic Calcium–Phosphate (Ca–P) coatings have been obtained on Titanium (Ti) substrates by the use of supersaturated solutions like Simulated Body Fluids (SBF) [1]. Such coatings are initiated by the heterogeneous nucleation of Ca–P globules. However, the formation of uniform Ca–P coating takes at least 7 days with regular refreshing of the solution [1–4]. The slowness of this process is due to the metastability of SBF at physiological conditions (37°C, pH = 7.25). In this study, a biomimetic Ca–P coating was obtained by soaking Ti6Al4V plates in a 5 times more concentrated SBF (so-called SBF × 5) with CO_2 gas [5–6]. This approach renders unnecessary refreshing the metastable solution, and it significantly accelerates the coating process. Our aim was to understand Ca–P nucleation mechanism towards Ti6Al4V substrate. Indeed, heterogeneous nucleation on a foreign substrate requires physical and chemical considerations. Several previous studies have shown that Ca–P have strong chemical and physical affinities for Ti substrate [5,7–13]. On one hand, Ca–P nucleation on Ti substrates is promoted by chemical affinities, which are related to surface charge of the Titanium oxide (TiO_2) layer that covers any Ti and alloys substrate [14–15]. On the other hand, the texture of the substrate can inhibit or promote, in vitro and in vivo, Ca–P nucleation depending on surface roughness [16–18]. Furthermore, we showed in a previous study that Ca–P coating crystallinity influences coating attachment and homogeneity on Ti6Al4V substrate: the lower HCO_3^- content in SBF × 5 was, the fewer the Ca–P developed on Ti6Al4V substrate [6]. The growing of small globules resulted in a more stable and homogeneous Ca–P coating. In this study, our aim was to investigate chemical and physical affinities that

*Corresponding author. IsoTis BV, PO Box 98, 3720 AB Bilthoven, Netherlands. Fax: +31-30-228-0255.
E-mail address: florence.barrere@isotis.com (F. Barrere).

0142-9612/02/$ - see front matter
PII: S0142-9612(01)00354-4

lead to Ca–P coating formation from SBF × 5 solution onto Ti6Al4V substrate. First, we analyzed our biomimetic Ca–P coating formed from SBF × 5 solution depth profile X-ray Photoelectron Spectroscopy (XPS) in order to enlighten favored Ca–P/Ti interactions. Second, since Magnesium (Mg^{2+}) is also known to inhibit apatite crystal growth [19–30], we studied its influence on Ca–P coating formation from SBF × 5 solution. We compared also its role with HCO_3^- ions role, since HCO_3^- lowers Ca–P coating crystallinity [6]. Therefore, we prepared several SBF × 5 solutions. On one hand, Mg^{2+} content was individually changed, whereas the other salts content remained similar to SBF × 5 solution composition. On the other hand, we prepared two additional solutions, in which one of the crystal growth inhibitor (Mg^{2+} or HCO_3^-) content was discarded and the other crystal growth inhibitor content was increased 8 times.

2. Materials and method

Ti6Al4V plates were ultrasonically cleaned successively in acetone, ethanol (70%) and finally demineralized water. These plates were then etched for 10 min in a mixture of 2 ml HF (40%) and 4 ml HNO_3 (66%) in 1000 ml of water. The average roughness (R_a) of the substrate was not affected by etching and remained at $R_a = 0.80\,\mu m$. Ti6Al4V plates were thereafter soaked into various SBF solutions (so-called SBF × 5). Composition of these various solutions is summarized in Table 1. Throughout the experiments, reagents grade chemicals were used (Merck). Each solution was prepared by dissolution of the salts into 1000 ml of demineralized water in which CO_2 gas was bubbled. The starting point of the experiments was set when CO_2 bubbling was stopped ($t = 0$ h). All the experiments were performed in a 1.5l-reactor thermostated at $37 \pm 1^{\circ}C$ for 24 h of soaking. The solutions were stirred with a magnetic bar with a speed of 200 rounds per minutes (rpm). pH of the calcifying solutions was recorded every 30 min with a combined electrode (pHmeter Portamess). Prior to experiments, the pH electrode was calibrated with two buffer solutions at pH = 4.01 and 7.00 (IUPAC standards, Radiometer Copenhagen). After 24 h of immersion Ti6Al4V plates were removed out of the SBF solution.

2.1. Qualitative and quantitative analysis of the biomimetic Ca–P by XPS depth profile

After 24 h of immersion into SBF × 5 solution, Ti6Al4V plates were taken out of the solution, ultrasonically cleaned with demineralized water, and finally dried at room temperature overnight. At the end of the experiment ($t = 24$ h) the precipitate formed in SBF × 5 solution was filtrated through a Whatman paper no. 5, and dried overnight in air at 50°C. Analysis of this precipitate was performed by Fourier Transform Infra-Red (FTIR, 8 scans, Perkin-Elmer, Spectrum 1000) and X-ray Diffraction (XRD, Rigaku Miniflex goniometer). X-rays were produced by a monochromatic source (Cu Kα, $\lambda = 1.54$ Å, 30 KV, 15 mA). XRD pattern was recorded as follows: scan range: $2\theta = 3.00$–60.00°, scan speed: 2.00°/min, scan step: 0.02°. Plates were microscopically investigated using Environmental Scanning Electron Microscopy with a Field Emission Gun (ESEM-FEG, Philips, model XL-30, 10 keV). The Ca–P coated Ti6Al4V plates were analyzed by XPS (Surface Science Instrument M-Probe, United Kingdom) using a monochromatized source using Al Kα. An XPS depth profile qualitative analysis was performed by gradually removing the coating with an Argon (Ar) Ion Etch Gun, calibrated at 3 nm/min. The detection limit of XPS depth profile analysis for atomic percentage was about 1%.

2.2. Influence of magnesium on the Ca–P coating formation

In order to investigate the role of magnesium (Mg^{2+}) in SBF × 5 various highly concentrated SBF solutions were prepared (see Table 1). SBF × 5(Mg × 0) was a Mg-free SBF × 5 solution. SBF × 5(Mg × 3) was a solution where Mg^{2+} was increased to 3 times as

Table 1
Inorganic composition (mM) of human blood plasma (HBP), regular Simulated Body Fluid (SBF), experimental SBF × 5 solutions

	NaCl	$MgCl_2 \cdot 6H_2O$	$CaCl_2 \cdot 2H_2O$	$Na_2HPO_4 \cdot 2H_2O$	$NaHCO_3$
HBP	146.7	1.5	2.5	1.0	27.0
SBF	146.7	1.5	2.5	1.0	4.2
SBF × 5	733.5	7.5	12.5	5.0	21.0
SBF × 5 (Mg × 0)	733.5	0.0	12.5	5.0	21.0
SBF × 5 (Mg × 3)	733.5	4.5	12.5	5.0	21.0
SBF × 5 (Mg × 8, HCO_3 × 0)	733.5	12.0	12.5	5.0	0.0
SBFx5 (Mg × 0, HCO_3 × 8)	733.5	0.0	12.5	5.0	33.6

compared with a regular SBF solution. The leftover salts concentrations remained similar to SBF × 5 solution. Furthermore, in order to differentiate the role of magnesium ions (Mg^{2+}) and hydrogenocarbonate ions (HCO_3^-), two additional solutions were prepared. SBF × 5 (Mg × 8, HCO_3 × 0) solution is an HCO_3-free solution with [Mg^{2+}] raised to 8 times as compared with regular SBF solution. Contrarily, SBF × 5(Mg × 0, HCO_3 × 8) solution is an Mg-free solution with [HCO_3^- was also raised to 8 times. Twenty Ti6Al4V plates were soaked in each solution (SBF × 5(Mg × 0), SBF × 5(Mg × 3), SBF × 5(Mg × 8, HCO_3 × 0) and SBF × 5(Mg × 0, HCO_3 × 8)). A kinetic study was performed for each experiment by measuring the pH of the solution, by taking out two Ti6Al4V plates every hour and by determining visually when the precipitation occurred in the solution. The presence of any Ca–P coating on the plates was checked with Energy Dispersive for X-ray analysis (EDX, Philips). Filtration and analysis of the Ca–P precipitates, gathered at the end of the experiments, were performed by FTIR and XRD as mentioned above. The removed Ti6Al4V plates were cleaned, dried and observed by ESEM as mentioned above.

3. Results

3.1. Qualitative and quantitative characterization of the biomimetic Ca–P obtained from SBF × 5 solution

As shown Fig. 1, pH of SBF × 5 solution raised from 5.9 at $t = 0$ h to 8.1 at $t = 24$ h. The XRD pattern of the precipitate exhibited two wide bumps located at about $2\theta = 30°$ and at $2\theta = 45°$. These bumps were characteristic of the broadening of apatitic diffraction lines indicating a poorly crystallized structure (Fig. 1b). The FTIR spectrum (Fig. 1c) corroborated previous XRD observations. Intense and broad bands assigned to O–H stretching and bending of H_2O were observed at, respectively, 3435 and 1646 cm^{-1}. Additionally, three bands at 1497 and 1428 cm^{-1} at 868 cm^{-1}were assigned to CO_3^{2-} groups. The broad and one-component bands at 1043 and 560 cm^{-1} corresponded to phosphate groups (PO_4^{3-}), while the band located at 868 cm^{-1} corresponded to HPO_4^{2-} groups. These featureless PO_4^{3-} bands were characteristic of a disordered environment. Therefore, the precipitate formed in SBF × 5 was a poorly crystallized or amorphous carbonated Ca–P phase. ESEM photos of the final coating after 24 h of immersion in SBF × 5 (Fig. 1d) indicated that a uniform

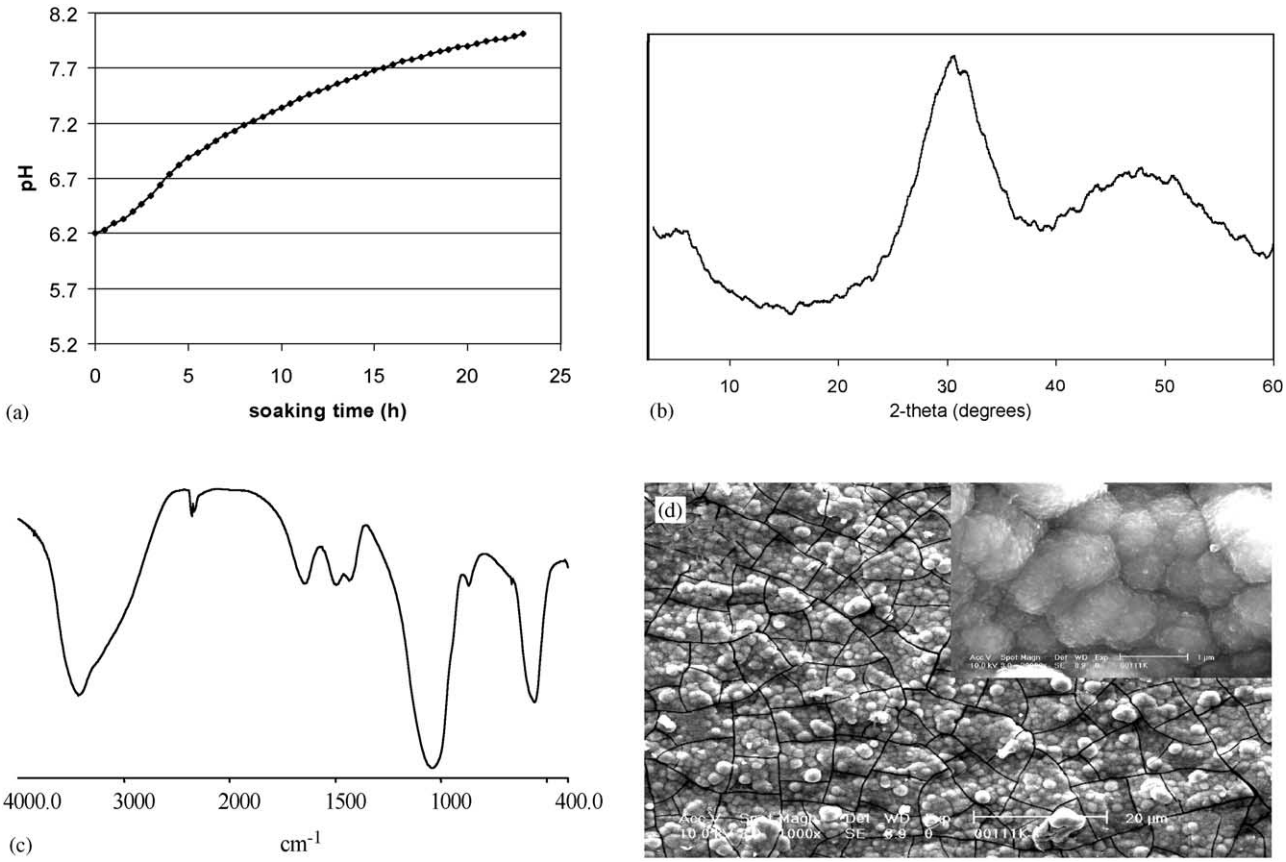

Fig. 1. SBF × 5 (a) pH versus soaking time, (b) XRD, (c) FTIR and (d) ESEM photos at magnification × 1000 and × 20000.

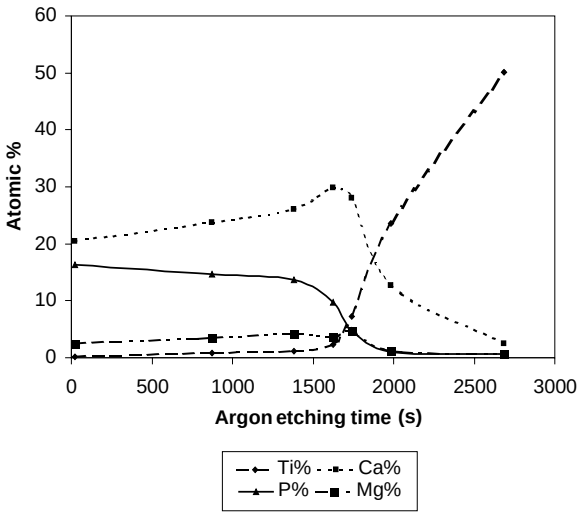

Fig. 2. XPS depth profile of the biomimetic Ca–P coating obtained from SBF × 5 solution. Atomic percentages of the elements (Calcium (Ca), Phosphorus (P), Magnesium (Mg), and Titanium (Ti)) are plotted versus Argon etching time (s).

Ca–P layer covered the plate as a dense Ca–P film composed of globules of 1–5 μm in size. At high magnification (×20000) the globules exhibited nanometric nuclei indicating that the film was composed of an amorphous or nano-crystalline compound. Fig. 2 shows the quantitative variation of the elements present in the Ca–P coated Ti6Al4V sample (Ca%, P%, Mg% and Ti%) versus cumulative Ar etching time, related to the depth analysis. Considering the depth profile, from 0 to 1383 s of etching, Ca, P and Mg are the main elements detected by XPS. P%, Ca% and Mg% remained quite stable at, respectively, 15.0%, 22.0% and 3.0%. This first part corresponded uniquely to Ca–P coating. Beyond 1383 s of etching, P%, Ca% and Mg% started to significantly evolve. For example, after 1623 s of etching, %P decreased to 9.8%, while the %Ca raised to a maximum of 29.8%, and %Mg remained stable at 3.7%. At this etching time, 1623s, the calculated atomic ratios were Ca/P = 3.0, Ca/Ti = 12.9 and P/Ti = 4.3. Deeper in the sample, at 1743 s, %Ti started to increase rapidly at 7.2%, indicating the approach of Ti6Al4V substrate, and corresponding to the coating/substrate interface. Considering the other elements after 1743 s of etching, %P, %Ca and %Mg were, respectively, 4.8%, 28.1% and 4.6%. Ca and Mg were highly present in comparison to P at the interface as indicated by the atomic ratios Ca/P = 5.9, Ca/Ti = 3.9 and P/Ti = 0.6. The high Ca/P ratio could not correspond uniquely to any Ca–P phase. For 1983 s of etching, %P, %Ca and %Mg continued decreasing, whereas %Ti increased to 23.6%. However a similar tendency was observed. %Ca and %Mg were still relatively high as compared with %P. Beyond 1983 s of etching, Ti was the main detectable element indicating the end of the interface, and herewith the unique Ti6Al4V substrate.

3.2. Influence of magnesium on the Ca–P coating formation

All the results concerning the kinetic study and the Ca–P structures are summarized Table 2.

3.2.1. SBF × 5(Mg × 0) and SBF × 5(Mg × 3)

Influence of magnesium content on Ca–P formation In the case of the Mg-free solution SBF × 5(Mg × 0), the starting pH was pH = 5.8 (Fig. 3a). During the first 6 h, the pH increased with a slope of 0.14 pH-units/h. At $t = 6$ h, the pH suddenly dropped from 6.8 to 5.7 within 30 min. Subsequently pH increased again and reached pH = 7.9 at $t = 24$ h. By $t = 6$ h during the pH drop, a precipitate appeared through the whole solution. XRD analysis of this precipitate gathered at $t = 24$ h exhibits quite broad diffraction lines (Fig. 3b). The position of these diffraction lines indicated an apatitic structure. The peak at $2\theta = 32.1^\circ$ corresponded to the overlapping of (2 1 1), (1 1 2), (3 0 0) and (2 0 2) diffraction plans. In addition the peak at $2\theta = 25.8^\circ$ corresponding to diffraction plan (0 0 2) of apatitic structure indicated

Table 2
Kinetics of precipitation and coating formations of the various experiments

Experiment	Precipitation formation		Coating formation		Precipitate structure	Slope (/h)
	pH	Time (h)	pH	Time (h)		
SBF × 5	6.7	$4\frac{1}{2}$	6.8	$5\frac{1}{2}$	$AmCO_3$–CaP[b]	0.11
SBF × 5 (Mg × 0)	6.7	6	/	/	CO_3–Ap[c]	0.14
SBF × 5 (Mg × 3)	6.7	4	6.8	$4\frac{1}{2}$	$AmCO_3$–CaP[b]	0.15
SBF × 5 (Mg × 8, HCO_3 × 0)	6.6	$15\frac{1}{2}$	6.6	$15\frac{1}{2}$	DCPD[a]	0.12
SBF × 5 (Mg × 0, HCO_3 × 8)	6.4	$1\frac{1}{2}$	7.0	10	CO_3–Ap/calcite	0.12

[a]DCPD: brushite.
[b]$AmCO_3$–CAP: amorphous carbonated CaP.
[c]CO_3–Ap: carbonated apatite.

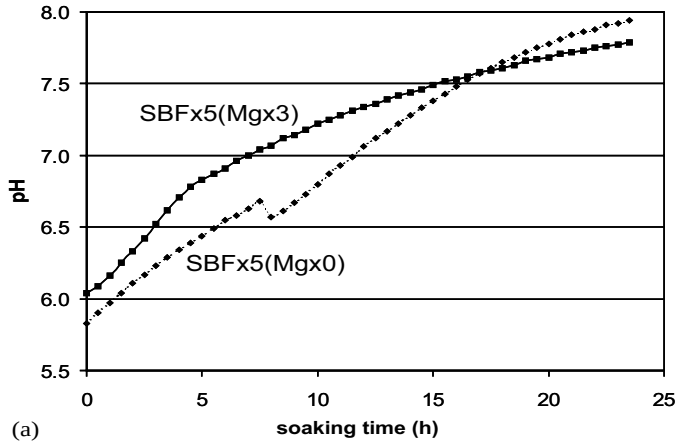

(a)

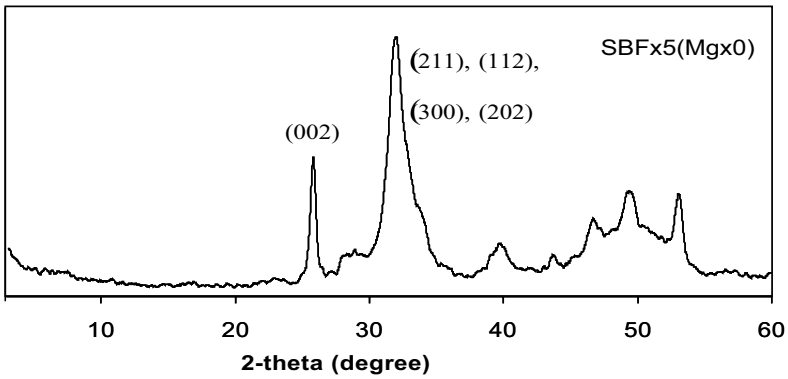

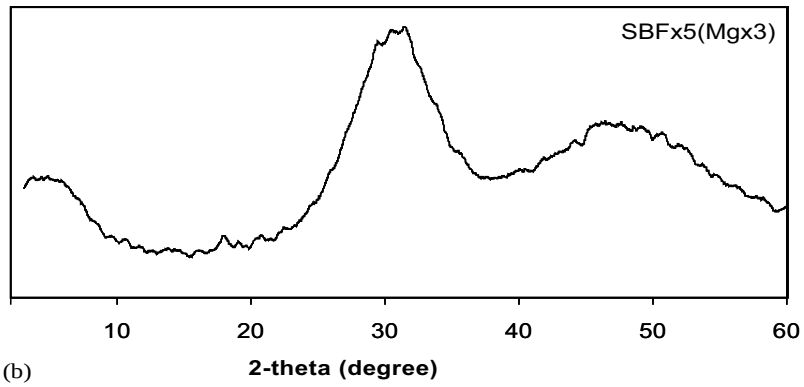

(b)

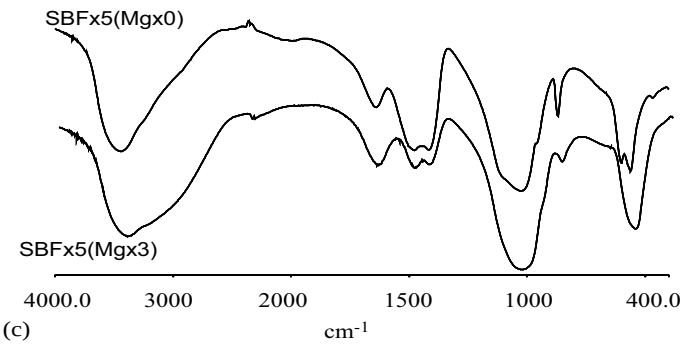

(c)

Fig. 3. SBF × 5 (Mg × 0) and SBF × 5 (Mg × 3) experiments (a) pH versus soaking time (b) XRD (c) FTIR and (d) ESEM photos at magnification × 1000 and × 20000.

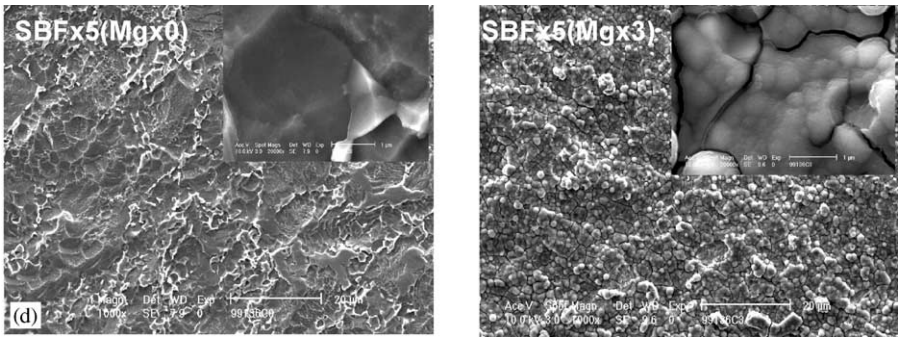

Fig. 3. (*Continued.*)

that SBF × 5 (Mg × 0) precipitate was composed of tiny apatitic crystals. The FTIR characterization confirmed this observation (Fig. 3c). The spectrum showed intense and broad bands assigned to O–H stretching and bending of H_2O (3435 and 1646 cm^{-1}), three bands corresponding to CO_3^{2-} groups (v_3 mode at 1497 and 1428 cm^{-1} and v_2 mode at 868 cm^{-1}). PO_4^{3-} groups were located at 1028 cm^{-1} (v_3 mode), at 960 cm^{-1} (v_1 mode) and at 602 and 563 cm^{-1} (v_4 mode). Furthermore HPO_4^{2-} groups were detected at 1108 cm^{-1} (v_3 mode). This indicated a Ca-deficient carbonated apatitic structure. Besides Ca–P precipitation in SBF × 5(Mg × 0) solution, Ti6Al4V surface did not exhibit any changes for 24 h of experiments. ESEM pictures of the removed Ti6Al4V plates did not show any Ca–P traces but only substrate texture (Fig. 3d). The EDX analysis of this sample only indicated Ti and Al peaks. Thereby, the immersion of the Ti6Al4V samples into SBF × 5 (Mg × 0) did not lead to the formation of any Ca–P trace on the substrate.

In the case of a SBF × 5(Mg × 3) ([Mg] = 4.5 mM), the starting pH is pH = 6.0. Within approximately the first 5 h, the pH increased rapidly with a slope of 0.15 pH-units/h. Subsequently, the pH slope was quite reduced. At the end of the experiments, pH reached 7.8 (Fig. 3a). A precipitate formed in the solution at $t = 4$ h (pH = 6.7). XRD and FTIR spectra (respectively, Fig. 3b and Fig. 3c) of the final precipitate gathered at the end of the experiments indicated a one-component and broad PO_4^{3-} IR bands and wide XRD bumps. In other words, the precipitate formed in SBF × 5(Mg × 3) is a poorly crystallized carbonated Ca–P structure. Simultaneously to precipitation ($t = 4\frac{1}{2}$ h, pH = 6.8), a colorful layer appeared on the Ti6Al4V plates corresponding to a Ca–P layer as indicated EDX analysis. By ESEM, at magnification × 1000, the final coating appeared dense and presented some cracks. This Ca–P coating covered uniformly the Ti6Al4V surface and it was composed of numerous Ca–P globules of ≈1–5 μm in diameter (Fig. 3d). At high magnification (× 20000), these globules were dense and they were composed of nano-metric globules. No crystals could be observed on Ti6Al4V substrate following its immersion in SBF × 5(Mg × 3).

3.3.2. *SBF × 5(Mg × 8, HCO_3 × 0) and SBF × 5(Mg × 0, HCO_3 × 8): Differentiation of carbonate and magnesium role*

In the case of SBF × 5(Mg × 8, HCO_3 × 0) ([Mg] = 12 mM, [HCO_3] = 0 mM), the starting pH was 5.3. During the first 3 h, the pH increased with a slope of 0.13 pH-units/h. At $t = 16$ h, pH reached a plateau at 6.6 (Fig. 4a). Meanwhile, a precipitation occurred into SBF × 5 (Mg × 8, HCO_3 × 0) solution. The XRD spectrum of this precipitate gathered at the end of the experiments exhibited sharp peaks indicating a highly crystallized structure (Fig. 4b). The diffraction lines at $2\theta = 11.7°$ and at $2\theta = 29.3°$ are characteristic of brushite (DCPD). FTIR spectrum (Fig. 4c) was in compliance with the previous XRD investigations, the phosphate and hydrogenophosphate bands are characteristic of DCPD structure (1220, 1134 1074, 1059, 1000 and 986 cm^{-1} for P–O v_3 mode, 874 cm^{-1} for P–O(H) v_1 mode and 525 cm^{-1} for P–O v_4 mode) (fig). Simultaneously to the precipitation into SBF × 5(Mg × 8, HCO_3 × 0) solution, a colorful Ca–P film was formed. At $t = 24$ h, ESEM photos of the final coating exhibited a dense and smooth morphology with some Ca–P globules of approximately 2 μm in diameter (Fig. 4d). At high magnification (× 20000), this smooth layer was composed of expanded globules containing nano-sized globules.

In the case of SBF × 5(Mg × 0, HCO_3 × 8) solution ([Mg] = 0 mM, [HCO_3] = 33.6 mM), the starting pH was 6.1 (Fig. 4a). During the first 3 h, the pH increased with a slope of 0.12 pH-units/h. Subsequently, pH dropped from 6.6 ($t = 2\frac{1}{2}$ h) to 6.4 ($t = 3$ h). Further, pH stared to rise and reached pH = 7.9. This pH remained stable until $t = 18\frac{1}{2}$ h. Subsequently, pH decreased again to pH = 7.8 at the end of the experiments ($t = 24$ h). At $t = 1\frac{1}{2}$ h (pH = 6.4), a precipitation occurred in SBF × 5(Mg × 0, HCO_3 × 8). The XRD pattern of the precipitate gathered at $t = 24$ h exhibited meanwhile sharp and broad diffraction lines (Fig. 4b). The sharp diffraction

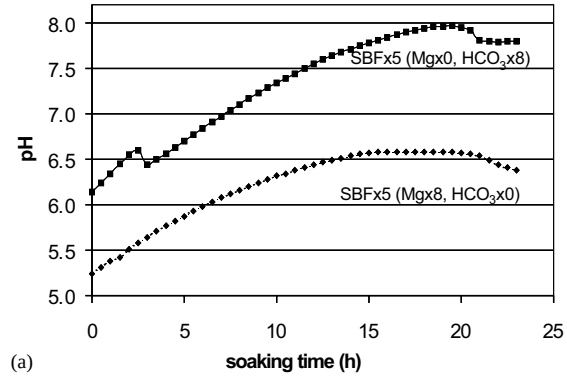

(a)

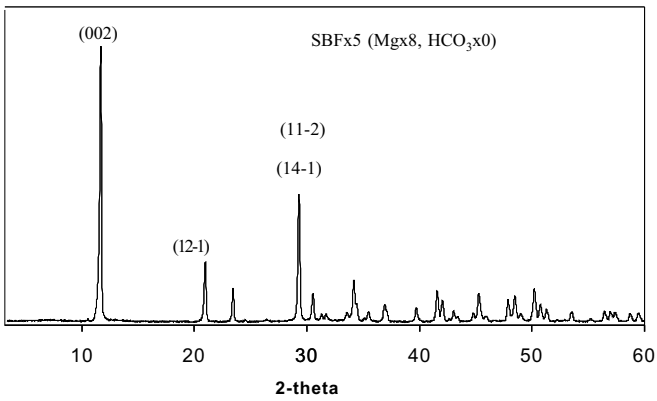

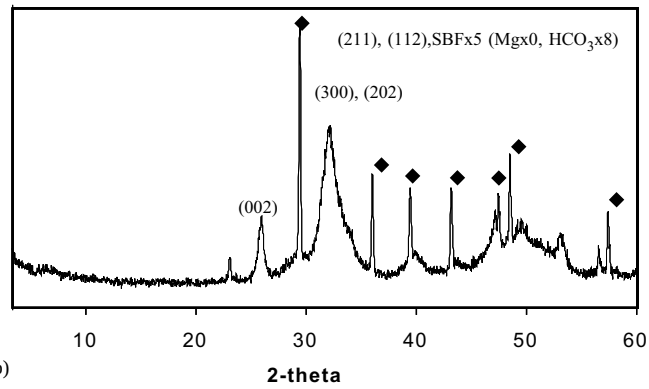

(b)

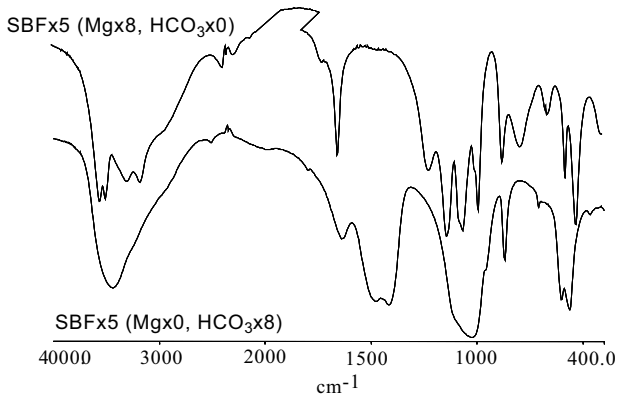

(c)

Fig. 4. SBF × 5 (Mg × 0, HCO_3 × 8) and SBF × 5 (Mg × 8, HCO_3 × 0) experiments (a) pH versus soaking time (h), (b) XRD, (c) FTIR and (d) ESEM photos at magnification × 1000 and × 20000.

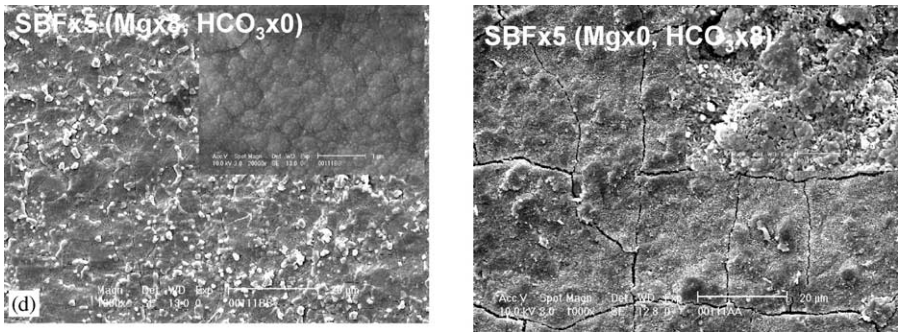

Fig. 4. (*Continued*).

lines could be assigned to calcite structure, whereas the broad diffraction lines could be assigned to apatitic structure where the peak at $2\theta = 32.06^\circ$ corresponded to the overlapping of (2 1 1), (1 1 2), (3 0 0) and (2 0 2) diffraction plans. Besides PO_4^{3-} groups located at $1028\,cm^{-1}$ (ν_3 mode), at $960\,cm^{-1}$ (ν_1 mode), at 602 and $563\,cm^{-1}$ (ν_4 mode) and HPO_4^{2-} groups at $1108\,cm^{-1}$ (ν_3 mode), FTIR spectrum of the precipitate (Fig. 4c) exhibited strong and large CO_3^{2-} bands at 1480 and $1416\,cm^{-1}$ (ν_3 mode) and at $868\,cm^{-1}$ (ν_2 mode) corresponding to carbonated Ca–P structure. Additionally two sharp and fine bands located at 1793 and $713\,cm^{-1}$ were assigned to calcite structure ($CaCO_3$). At $t = 10\,h$ (pH = 7.0), a whitish layer covered uniformly the Ti6Al4V substrate. EDX of this layer indicated the formation of a Ca–P film. At the end of the experiments, the ESEM photos of the final sample revealed an heterogeneous coating morphology (Fig. 4d). The coating seemed to be first covered with tiny crystals. These crystals were partially covered by nano-sized globules. Though calcite was detected in the precipitate, the microstructure of this coating suggested the formation of Ca–P compounds on the Ti6Al4V substrate rather than $CaCO_3$.

4. Discussion

4.1. Role of magnesium in SBF × 5 solution

From the overall experiments, Mg^{2+} strongly affects the Ca–P coating formation and structure. This important effect is emphasized by XPS depth profile of the final Ca–P coating obtained from SBF × 5 solution. As previously shown [6], immersion of Ti6Al4V plates into SBF × 5 led to the deposition of a uniform and thin amorphous carbonated Ca–P layer within $5\frac{1}{2}\,h$. This coating, together with a precipitate, formed while CO_2 gas is released out of the solution. This CO_2 release induces a pH raise leading to an increasing supersaturation of SBF × 5 solution and, to Ca–P nucleation in the solution and onto the Ti substrate. Mg^{2+} affects Ca–P coating process at different stages, related to its Ca–P crystal growth inhibitory effect [19–21, 27]. When Mg^{2+} is lowered, pH curve is affected. As discussed elsewhere, CO_2 release prevented the drop in pH that is usually observed during Ca–P formation [6]. In the particular case of Mg-free SBF × 5 solutions (SBF × 5(Mg × 0) and SBF × 5(Mg × 0, HCO_3 × 8)), pH suddenly decreases simultaneously to precipitation in the solution. When Mg^{2+} is absent of SBF × 5 solution, Ca–P precipitation occurs suddenly, leading to a drop in pH. Kibalczyc et al. have already reported dependence of pH drop versus the amount of Mg^{2+} contents: higher Mg^{2+} content is, smaller is the pH drop [24]. pH decreases slower in the case of Mg-containing SBF solutions as compared with Mg-free SBF solutions. Additionally, in our experiments, pH decrease is prevented by CO_2 release leading to a pH increase. When Mg^{2+} content is increased in SBF × 5 solution, Ca–P precipitation is delayed and the precipitate structure is changed into amorphous or poorly crystallized apatite. Indeed Mg^{2+} is known to poison Ca–P surfaces by disturbing the crystal growth process and by stabilizing amorphous Ca–P phases in detriment to apatitic phases [24–30]. When SBF × 5 solutions are supersaturated towards apatite and Mg^{2+} content increases, the crystallinity of the precipitate decreases. In the particular case of SBF × 5(Mg × 8, HCO_3 × 0), the precipitate has a highly crystallized DCPD structure. It appears that Mg^{2+} does not affect DCPD formation as it was already shown by previous studies [20–21, 30]. As Mg^{2+} affects precipitate structure, it strongly affects coating formation as well. When comparing coatings obtained from SBF × 5(Mg × 3) and from SBF × 5, Ca–P globules were larger with low Mg^{2+} content. When Mg^{2+} content is increased in SBF × 5(Mg × 8, HCO_3 × 0) solution, though without HCO_3^-, the coating is evenly composed of smaller globules. This difference in size is obviously due to inhibitory effect of Mg^{2+} as mentioned above. On the other hand, when Mg^{2+} content is removed from SBF × 5 solution, no Ca–P trace was detected on Ti6Al4V substrate. This experiment suggests that Mg^{2+} is essential for Ca–P coating

formation. At this stage three hypotheses can be considered. First, Ca–P crystals might have been too large to remain on Ti6Al4V substrate. Due to a lack of Mg^{2+}, Ca–P crystals could have grown as it partially happened in the case of HCO_3-free SBF × 5 solution as published previously [6]. Secondly, due to the absence of Mg^{2+}, precipitation occurs suddenly in the solution. Consequently, the energy required to grow Ca–P homogeneously in the solution is lower than energy required for heterogeneous nucleation on the substrate. These two last hypotheses can be supported by experiment SBF × 5($Mg \times 0$, $HCO_3 \times 8$). Despite the absence of Mg^{2+} in this solution, a Ca–P coating was deposited on Ti6Al4V substrate. So, it would suggest that Mg^{2+} has a stronger inhibitory effect than HCO_3^- in our SBF × 5 conditions since a previous study [6] showed that, despite the absence of HCO_3^-, Ca–P formed on Ti6Al4V substrate. The non-uniformity of this coating is thought to be due to too large crystals grown on a flat substrate. However our first hypothesis seems rather unlikely improbable since Ti6Al4V plates were analyzed every hour and any Ca–P trace had never been detected. In a third hypothesis, additionally to a comparable tailoring effect of both HCO_3^- and Mg^{2+}, Mg^{2+} seems to have an important role at the Ca–P coating/substrate interface. Indeed, XPS depth profile of this thin Ca–P coating formed from SBF × 5 solution indicated that, like Ca%, Mg% reaches its maximum at the interface. This suggests that the coating formation was initiated by positive ions certainly due to a negatively charged TiO_2 surface. Because the isoelectric point of this TiO_2 layer is approximately pH = 6.0–6.2 [14–15], in the case of SBF × 5 solution the Ti6Al4V substrate is slightly negatively charged. Via the passive TiO_2 layer therefore, cationic species like Ca^{2+} and Mg^{2+} are preferably attracted. The high Mg^{2+} content at the vicinity of Ti6Al4V substrate inhibits Ca–P growth favoring tiny Ca–P globules on Ti6Al4V substrate. So the Ca–P coating, being composed of tiny globules, is stabilized on evenly smooth Ti6Al4V substrate.

4.2. General scheme of Ca–P coating formation from SBF × 5 solution

This study of Mg^{2+} role on Ca–P coating deposition on Ti6Al4V from SBF × 5 solution clarifies the Ca–P coating formation process. From a previous publication we have established that Ca–P formation in the solution and on the substrate, must be simultaneous in order to balance both phenomena [6]. Precipitation must not occur too fast in order to allow nucleation on substrate. Additionally HCO_3^-, like Mg^{2+}, reduces apatitic crystal growth. Consequently, both these ions reduce Ca–P crystal size and thereby, Ca–P crystals remain more stabilized on the flat Ti6Al4V substrate. Theoretically, heterogeneous nucleation on a substrate requires chemical and physical affinities, and Mg^{2+} in SBF × 5 solution seems to influence on both chemical and physical affinities. Indeed, in our study, cationic species, i.e. Ca^{2+} and Mg^{2+} are favorably attracted onto the TiO_2 passive layer covering Ti6Al4V plates. Both affinities towards Ca–P nucleation onto Ti and alloys have been already widely studied [5–11]. It is not clear yet to which extend each parameter, physical or chemical affinity, is important. For example, chemical treatments have been performed on Ti substrates in order to accelerate the Ca–P nucleation process [31–33]. These drastic treatments affect both surface composition as well as surface roughness. So it is ambiguous to evaluate at which extend, each parameter influences Ca–P nucleation. In our experiments, surface texture is kept similar throughout all the experiments. We only change ionic composition of SBF × 5. We hypothesize that the initial Ca–P nucleation step is primarily favored by chemical affinity. Li compared the ability of various substrates on Ca–P formation. The author has shown that alumina substrates, positively charged at pH = 7.4 do not initiate any Ca–P nuclei whereas silica and titania substrate lead to Ca–P nucleation due to their negatively charged surface at pH = 7.4 [8]. Concerning the nature of chemical bonding between Ca–P and Titanium remains quite ambiguous. Titanium substrate is believed to be negatively charged at physiological pH, whereas results show evidences for chemical affinities between Ti and HPO_4^{2-} [5,7,9,11] but rarely Ti and Ca^{2+} [5,9]. We think that these two kinds of affinities actually can be possible, and occur during Ca–P coating formation on Ti6Al4V [5]. All the aforementioned studies have been performed under different conditions of soaking solutions and analysis. This enables a definitive conclusion concerning a general scheme of chemical bonding. Concerning the physical affinity, it appears that the stability of this Ca–P coating is related to Ca–P globule development kinetics on the Ti6Al4V substrate. The uniform Ca–P coatings obtained in our experiments exhibit globules being amorphous or nano-crystalline as suggested FTIR and XRD analyses of the precipitates. These globules seem to have expanded during the formation process all over the surface to finally link with surrounding Ca–P globules growing as well. When Ca–P crystals were detected by ESEM, the Ca–P coating was heterogeneous due to the detachment of the largest Ca–P crystals. Thereby, in order to create a stable biomimetic Ca–P coating, this coating must first be composed of tiny Ca–P globules. The presence of Mg^{2+} present at the vicinity of the negatively charged surface inhibits apatite crystal growth in favor to poorly crystallized Ca–P globules. This leads to a strong attachment of the Ca–P coating on Ti6Al4V substrate.

5. Conclusion

The use of a five times more concentrated SBF solution allows the deposition of an homogeneous Ca–P coating within 24 h. The formation and attachment of this coating is strongly related to Mg^{2+} content. Indeed, Mg^{2+} is a key-factor for Ca–P coating formation from SBF × 5 solution. It inhibits precipitation in the solution and it favors the formation of Ca–P coating due to its relatively high concentration at the coating/substrate interface.

References

[1] Kokubo T, Kushitani H, Sakka S, Kitsugi T, Yamamuro T. Solutions able to reproduce in vivo surface-structure changes in bioactive glass-ceramics A-W^3. J Biomed Mater Res 1990;24:721–34.

[2] Li P, Kangasniemi I, de Groot K, Kokubo T. Bonelike hydroxyapatite induction by a gel-derived titania on a titanium substrate. J Am Ceram Soc 1994;77:1307–12.

[3] Peltola T, Patsi M, Rahiala H, Kangasniemi I, Yli-Urpo A. Calcium phosphate induction by sol-gel-derived titania coatings on titanium substrates in vitro. J Biomed Mater Res 1998;41: 504–10.

[4] Li P, Ducheyne P. Quasi-biological apatite film induced by titanium in a simulated body fluid. J Biomed Mater Res 1998;41:341–8.

[5] Barrere F, Layrolle P, van Blitterswijk CA, de Groot K. Fast formation of biomimetic Ca–P coatings on Ti6Al4V. Mater Res Soc Symp Proc 2000;599:135–40.

[6] Barrere F, van Blitterswijk CA, de Groot K, Layrolle P. Influence of ionic strength and carbonate on the Ca–P coating formation from SBF × 5 solutions. Biomaterials 2002;23:1921–30.

[7] Combes C, Freche M, Rey C. Nucleation and crystal growth of dicalcium phosphate dihydrate nucleation on titanium powder. J Mater Sci: Mater Med 1995;6:699–702.

[8] Li P. In vitro and in vivo calcium phosphate induction on gel oxide. Ph.D. thesis, Leiden university, 1993.

[9] Healy KE, Ducheyne P. Hydration and preferential molecular adsorption on titanium in vitro. Biomaterials 1992;13:553–61.

[10] Ong JL, Lucas LC. Auger electron spectroscopy and its use for characterization of titanium and hydroxyapatite surface. Biomaterials 1998;19:455–64.

[11] Hanawa T. Titanium and its oxide film: a substrate for formation of apatite. In: Davies JE, editor. The bone-biomaterial interface. University Toronto Press, Toronto, Canada, 1990. p. 49–61.

[12] Yan WQ, Nakamura T, Kobayashi M, Kim HM, Miyaji F, Kokubo T. Bonding of chemically treated titanium implants to bone. J Biomed Mater Res 1997;37:267–75.

[13] Combes C, Rey C, Freche M. XPS and IR study of dicalcium phosphate dihydrate nucleation on titanium surface. J Coll Surf B: Biointerfaces 1998;11:15–27.

[14] Thull R. In: Helsen JA, Breme HJ, editors. Metals as biomaterials. England: Wiley, 1998. p. 291–315.

[15] Tengvall P, Lundström I. Physico-chemical considerations of titanium as a biomaterial. Clin Mater 1992;9:115–34.

[16] Leitao E, Barbosa MA, de Groot K. Influence of substrate material and finishing on the morphology of the Calcium–Phosphate coating. J Biomed Mater Res 1997;36:85–90.

[17] Buser D, Schenk RK, Steinemann S, Fiorellini JP, Fox CH, Stich H. Influence of surface characteristics on bone integration of titanium implants. A histomorphometric study in miniature pigs. J Biomed Mater Res 1991;25:889–902.

[18] Thomas KA, Cook SD. An evaluation of variables influencing implant fixation by direct bone apposition. J Biomed Mater Res 1985;19:875–901.

[19] Tomazic B, Tomson M, Nancollas GH. Growth of calcium phosphates on hydroxyapatite crystals: the effect of magnesium. Arch oral Biol 1975;20:803–8.

[20] Salimi MH, Heughebaert JC, Nancollas GH. Crystal growth of calcium phosphates in the presence of magnesium ions. Langmuir 1985;1:119–22.

[21] Eanes ED, Rattner SL. The effect of magnesium on apatite formation in seeded supersaturated solutions at pH = 7.4. J Dent Res 1980;60:1719–23.

[22] Termine JD,R, Peckauskas RA, Posner AS. Calcium phosphate formation in vitro. II Effect of environment on amorphous-crystalline transformation. Arch Biochem Biophys 1970;140: 318–25.

[23] Martens CS, Harriss RC. Inhibition in the marine environment by magnesium ions. Geochim Cosmochim Acta 1970;34:621–5.

[24] Kibalczyc W, Christoffersen J, Christoffersen MR, Zielenkiewicz A, Zielenkiewicz W. The effect of magnesium ions on the precipitation of calcium phosphates. J Cryst Growth 1990;106:355–66.

[25] Newesely H. Changes in crystal types of low solubility calcium phosphates in the presence of accompanying ions. Arch Oral Biol 1961;6:SS174–80.

[26] Boskey AL, Posner AS. Magnesium stabilization of amorphous calcium phosphate: a kinetic study. Mater Res Bull 1974;9: 907–16.

[27] Nancollas GH, Tomazic B, Tomson M. The precipitation of calcium phosphate in the presence of magnesium. Croat Chem Acta 1976;48:431–8.

[28] Bachara BN, Fisher HRA. The effect of some inhibitors on the nucleation and crystal growth of apatite. Calcif Tissue Res 1969;3:348–57.

[29] Blumenthal NC. Mechanism of inhibition in calcification. Clin Orthop Relat Res 1989;247:279–89.

[30] Abbona F, Lundager Madsen HE, Boistelle R. The initial phases of calcium and magnesium phophates precipitated from solutions of high to medium concentrations. J Cryst Growth 1986;74: 581–90.

[31] Wen HB, Wolke JGC, de Wijn JR, Cui FZ, de Goot K. Fast precipitation of calcium phosphate layers on titanium induced by simple chemical treatment. Biomaterials 1997;18:1471–8.

[32] Kim HM, Miyaji F, Kokubo T, Nakamura T. Preparation of bioactive Ti and its alloys via simple chemical surface treatment. J Biomed Mater Res 1996;32:409–17.

[33] Ohtsuki C, Iida H, Hayakawa S, Osaka A. Bioactivity of titanium treated with hydrogen peroxide solutions containing metal chloride. J Biomed Mater Res 1997;35:39–47.